GaN-based Robot Power Supply Design

Jie Gan[1,3], Mohd Azli Bin Salim[2] and Chonlatee Photong[3,*]

[1] Faculty of Electrical Engineering, Guangxi Technological College of Machinery and Electricity, No.101, DaXueDongLu Road, Nanning, Guangxi, China
[2] Smart Manufacturing and Innovation Centre, Universiti Teknikal Malaysia Melaka, Melaka, Malaysia
[3,*] Faculty of Engineering, Mahasarakham University, Khamriang Sub-District, Kantarawichai District, Maha Sarakham 44150, Thailand (Corresponding Author)

imganjie@gmail.com, azli@utem.edu.my and chonlatee.p@msu.ac.th[*]

Abstract. *The purpose of this paper is to report how a combination of a totem-pole bridgeless PFC converter and an LLC converter can achieve a high-efficiency power supply operating at 500 kHz, and to compare the stress and losses in the circuit between the proposed GaN-based and conventional Si-based devices. From the experimental point of view, under the proposed topology, the operating loss of the Si-based devices (21.98W) was higher than that of the GaN-based device (4.13W), and the power supply could reach 97.5% efficiency.*

Received by	21 June 2022
Revised by	30 July 2022
Accepted by	19 September 2022

Keywords:

GaN semiconductor devices, power supply design, robotics, totem-pole bridgeless PFC, LLC converter

1. Introduction

There are a number of robots increasing nowadays due to the fast growth of Artificial Intelligent (AI) that has improved many operations of machines and is widely adopted in industries such as medical, healthcare, service, hospitality, and manufacturing. This is because of the fact that these robots and machines have been employed to perform humans operations during this industrial revolution worldwide [1].

Electricity as clean energy [2], one of the most important parts of the robots is the power supply that helps to convert supplying power into the most suitable amount and levels. A high power rating power supply would provide more robust and retain greater power conversion compared to a low power rating power supply. But would encounter some problems related to the investment costs, power losses, larger size, and heavier weight. As a result, this causes the crucial demand for optimum mobility and miniaturization that has led to the development of miniaturization of the various modules of the robots. In addition, the volume of the power module is also a major factor that restricts the volume and portability of the robots. Due to the fact that the volume and heat dissipation limitations of the power device. Therefore, designing a power supply with high efficiency, small size, and low heat generation is particularly important for the development of the robotics industry.

In these recent years, the GaN-based power electronic devices would possibly be used to replace the conventional Si-based ones used nowadays due to their higher power density rating, smaller size, and lighter weight. There are some research works that have been studied on these devices available in the literature [3]-[10]. But performance in terms of efficiency and performance compared to the Si-based devices has not been properly compared.

The diode-bridge AC-DC power factor correction (PFC) converters could increase power losses in the circuits. Therefore, bridgeless AC-DC converters are ones of the particular interesting topology to reduce the losses and hence increase the power conversion efficiency. The PFC converters are suitable for up to 230Vac input voltage and up to 400Vdc output voltage applications. There have been many articles comparing PFC topologies [11]-[14], and the results showed that in high frequency applications, the totem pole PFC topology is more advantageous.

The LLC resonant converters [15]-[20] are considered as the DC-DC converters to regulate the voltage across the battery. These converters are very popular due to the capability of zero voltage switching over a wide input voltage range with relatively low switching losses. Hence, the second fundamental frequency ripple at the PFC converter output (380-400V) can be regulated to 48V for battery charging applications by the LLC converters. Another advantage of these converters are the soft-switching operation in the entire load range [21].

In this research, the comparison of GaN-based switching devices for the most suitable totem-pole bridgeless circuit for the AC-DC power converter and the LLC circuit for the DC-DC power converter when used as the commercial mobile robot power supply adaptors in terms of stresses, losses are examined compared with the conventional Si-based switching devices. The results from simulation tests will be used to validate the research study.

2. Design of Totem-Pole Bridgeless PFC with LLC Converter Topology

The totem-pole bridgeless PFC circuit consists of very few components in the circuit and only one diode is on during half an operating frequency cycle, which therefore has very low losses [22],[23]. The totem-pole bridgeless PFC circuit S_1 and S_2 body diodes work in high frequency on and off states to play the role of current renewal, so the totem-pole bridgeless PFC circuit has high requirements for the reverse recovery characteristics of S_1 and S_2 body diodes. S_1 and S_2 if using Si MOSFET, due to the poor reverse recovery characteristics of Si MOSFET body diodes, and thus would generate high power losses. This is enough to offset the low loss advantage of the totem-pole bridgeless PFC circuit, which will be compared with the loss of the Si-based devices and GaN-based devices in subsequent sections of this paper.

The advantage of the LLC resonant converters is that all devices can achieve zero voltage switching (ZVS) over the entire load range and zero current switching (ZCS) for the secondary side devices when the converter is operating at the resonant point [17]. Therefore, the LLC resonant converters are well suited for small to medium power high switching frequency converters.

The model discussed in this paper is a power supply model without EMI, the block diagram of the proposed PFC converter with a LLC circuit is shown in Fig. 1 while the actual circuit configuration used in this paper is shown in Fig. 2.

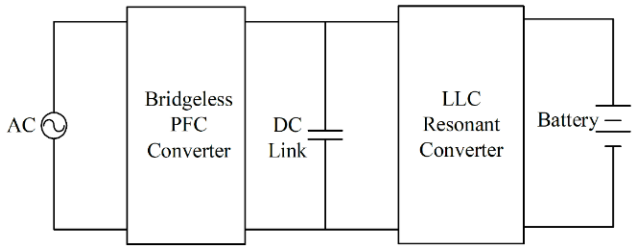

Fig. 1 The block diagram of the proposed converter

The proposed totem-pole bridgeless PFC converter with a LLC resonant converter was designed such that a low voltage battery of 48V could be charged from the ac source of 230V. The totem-pole bridgeless PFC converter with a LLC resonant converter was simulated at the operating frequency of 500 kHz and output power was 500W. The similar characteristics and specifications of the GaN HEMTs and Si MOS devices were used in the simulation of the proposed converter. The detailed design of the parameters and control strategy of the proposed converter is discussed in the next section.

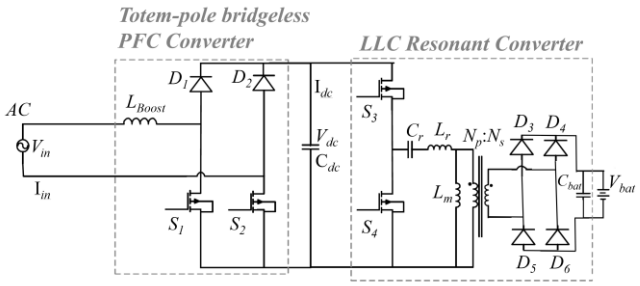

Fig. 2 The converter configuration of the proposed system

3. Design of the Converter Parameters

3.1 Design of the Totem-Pole bridgeless PFC Converter Parameters

The equations used for designing the parameters for the proposed totem-pole bridgeless PFC converter with a LLC converter were expressed by the equations (1) – (7) in accompanied with their examples of the calculated values as follows:

Determine the maximum average output current ($I_{OUT(max)}$) from the maximum output power ($P_{OUT(max)}$) and the dc-link voltage ($V_{DC\text{-}link}$) as equation (1):

$$I_{out(max)} = \frac{P_{out(max)}}{V_{DC\_link}} = \frac{550}{385} = 1.43A \quad (1)$$

The maximum input RMS line current, $I_{in\text{-}RMS(max)}$, could be calculated by using (2); where $P_{dc\text{-}OUT(max)}$ is the dc output power, η_{PFC} is the estimated efficiency of the PFC converter, $V_{IN(min)}$ is the minimum input voltage and PF is the estimated power factor:

$$I_{in\_rms(max)} = \frac{P_{dcOUT(max)}}{\eta_{PFC} \times V_{IN(min)} \times PF} = \frac{550}{0.99 \times 100 \times 0.98} = 5.67A \quad (2)$$

To determine the boost inductor (L_{boost}), the maximum-allowed ripple current ($I_{in\text{-}ripple\ (max)}$) was calculated first. The maximum ripple current was observed at the lowest input voltage and maximum load. Assuming a maximum 40% ripple in the inductor current, the ripple current could be calculated as follows:

$$I_{in\_ripple(max)} = \Delta ripple \times I_{in_{rms(max)}} = 0.4 \times \sqrt{2} \times 5.67 = 3.2A \quad (3)$$

The duty cycle ($DUTY_{(max)}$) at the peak of the minimum input voltage could be calculated as:

$$DUTY_{(max)} = \frac{V_{dc(max)} - \sqrt{2}V_{in(min)}}{V_{dc}} = \frac{385V - \sqrt{2} \times 100}{385} = 0.63 \quad (4)$$

The minimum value of the boost inductor (L_{boost}) was calculated based on the acceptable ripple current, at a worst-case duty cycle of 0.63, as expressed by (5):

$$L_{Boost} \geq V_{dc(max)} \times DUTY_{(max)} \times \frac{1 - DUTY_{(max)}}{F_{SW} \times I_{INripple(max)}}$$
$$= 385 \times 0.63 \times \frac{1-0.63}{500000 \times 3.2} = 560\mu H \quad (5)$$

The output capacitor (C_{dc}) was determined to meet the allowable DC link ripple and hold up the requirements of the converter. The ripple of DC link voltage could be calculated by using (6):

$$V_{ripple} = \frac{P_{dcOUT} \times 0.0032}{C_{dc} \times V_{dc}} \quad (6)$$

The holdup time required by this design, T_{Holdup} was 2ms. The average bus voltage was set at 385V, which was correlated with the LLC transformer ratio. Considering the DC link voltage has a +/-10V ripple at the full load, the DC bus voltage ($V_{dc(norm)}$) would be 365V in the valley point. Considering the gain of the LLC circuit that could not be too wide, the minimum input voltage of the LLC circuit ($V_{dc(min)}$) was set at 320V. For energy, the minimum value of the bus capacitance could be calculated using (7).

$$C_{dc} \geq 2 \times P_{dcOUT(norm)} \times \frac{T_{Holdup}}{V_{dc(norm)}^2 - V_{dc(min)}^2}$$
$$= 2 \times 500 \times \frac{0.002}{365^2 \times 320^2} = 649\mu F \quad (7)$$

3.2 Design of the LLC Resonant Converter Parameters

The equations used for designing parameters for the LLC Resonant Converter were given in the equations (8)–(18).

From the nominal input voltage ($V_{dc\text{-}nom}$), the transformer turns ratio (n) could be determined from (8):

$$n = \frac{V_{dc\_nom}}{2 \times (V_o + V_F)} = \frac{385}{2 \times (48 + 0.01)} \approx 4 \quad (8)$$

The required gain (M) at minimum and maximum input voltage could be determined using (9) and (10):

$$M_{min} = \frac{n \times (V_o + V_F)}{V_{dc\_max}/2} = \frac{4 \times (48 + 0.01)}{395/2} = 0.972 \quad (9)$$

$$M_{max} = \frac{n \times (V_o + V_F)}{V_{dc\_min}/2} = \frac{4 \times (48 + 0.01)}{320/2} = 1.2 \quad (10)$$

In the equations (8)-(10), V_F was a secondary side voltage drop.

Calculate the equivalent load resistance (R_e):

$$R_e = \frac{8n^2}{\pi^2} \times \frac{V_o}{I_o} = \frac{8 \times 4^2}{\pi^2} \times \frac{48}{11} = 56.6\Omega \quad (11)$$

The resonant circuit was composed of the resonant capacitor C_r and resonant inductor L_r. These resonant parameters could be calculated from (12) and (13):

$$C_r = \frac{1}{2\pi Q_e f_r R_e} \quad (12)$$

$$L_r = \frac{1}{(2\pi f_r)^2 C_r} \quad (13)$$

In this design, L_r=19μH and C_r=66nF were chosen for the circuit.

The magnetizing inductance (L_m) could be calculated from (14):

$$L_m = m \times L_r \quad (14)$$

From (14), m was referred as a ratio of L_m and L_r. Smaller m values could result in higher peak gains, but too small m values could, in turn, cause poor transformer coupling and reduce efficiency. Generally, the m value should be taken between 3 and 7.

In a real transformer, the resonant inductance could be integrated into the transformer, and the primary coil inductance (L_p) was equal to:

$$L_p = L_m + L_r \quad (15)$$

For an integrated transformer, the actual turns ratio of the transformer (n_{real}) could be calculated by using (16):

$$n_{real} = n\sqrt{\frac{L_r + L_m}{L_m}} \quad (16)$$

The secondary and primary side turns (N_s and N_p) could be calculated by using (17) and (18):

$$N_s = \frac{V_o + V_F}{4 f_{min} \times \triangle B \times A_e} \quad (17)$$

$$N_p = N_s \times n_{real} \quad (18)$$

In this design, N_p: N_s=18:5.

4. Computer Model Simulation

Considering that the subsequent analysis that was needed to use the GaN and Si MOSFETs for the simulation comparison analysis, all parameters were therefore set with the consistent. The values for the input indicators of the power supply and the related main power device parameters were defined as shown in Table 1.

Symbol	Parameter	Specifications
V_{in}	Input voltage	(100-264) V
$P_{out\ (nom)}$	Output Power	500 W
f_{sw}	Switching Frequency	500 kHz
L_{boost}	Iutput Current Ripple Inductor	1000 uH
C_{dc}	DC link capacitor	660 uF
V_{dc}	DC link voltage	(320-395) V
C_r	Resonant Capacitor	2x47 nF
L_r	Resonant Inductor	20 uH
N_{ps}	Secondary and Primary Side Turns	18:5
V_{bat}	Output Voltage	48 V

Table 1 Simulation main parameter specifications

The totem-pole bridgeless PFC converter simulation circuit and the LLC converter simulation circuit based on the parameters from Table 1 are shown in Fig.3 and Fig.4.

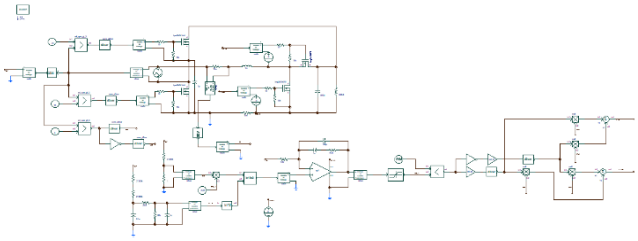

Fig. 3 the totem-pole bridgeless PFC simulation circuit

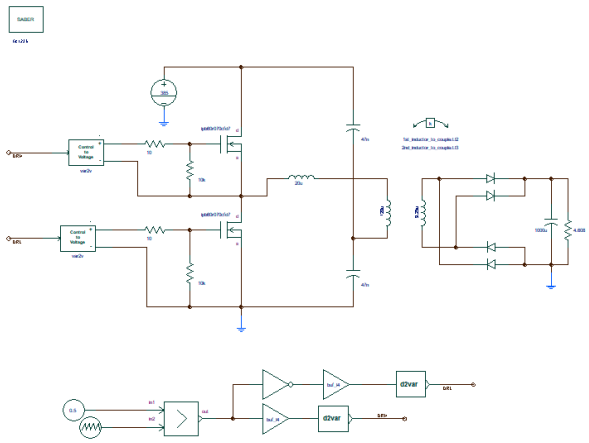

Fig. 4 the LLC resonant simulation circuit

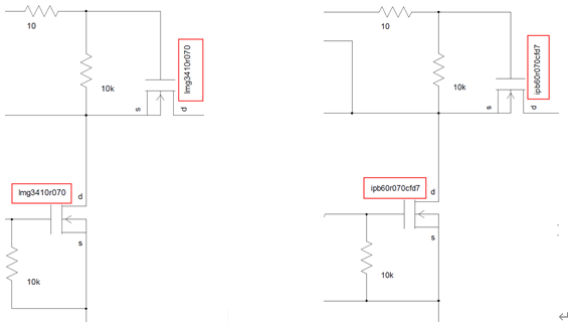

(a) (b)

Fig. 5 Simulation schematic diagram details comparison between (a) GaN HEMT (LMG3410R070) and (b) Si MOS (IPB60R070CFD7)

Symbol	Parameters	Semiconductor Devices	
		Si MOS (IPB60R070CFD7)	GaN HEMT (LMG3410R070)
V_{DS}	Drain-to-Source Voltage	600 V	600 V
$R_{DS(ON)}$	Drain-to-Source On Resistance	70 mΩ	70 mΩ
Q_G	Total Gate Charge	67 nC	4.5 nC
$CO_{(ER)}$	Effective Output Capacitance Energy Related	96 pF	95 pF
$CO_{(TR)}$	Effective Output Capacitance Time Related	990 pF	145 pF

Table 2 Comparison of key parameters between GaN HEMT (LMG3410R070) and Si MOS device (IPB60R070CFD7).

Fig.5 is an enlarged view of the simulation circuit device replacement, Table 2 shows the key parameters comparison between the GaN HEMT (LMG3410R070) [24] and the Si MOS device (IPB60R070CFD7) [25].

5. Results and Discussions

In this section, various simulations are performed using Synopsys Saber 2012 software, and the simulation results are discussed.

5.1 Comparison of the Outputs

Comparison of the Totem-Pole Bridgeless Circuit Outputs, Fig.6(a) is the output voltage and current waveforms using the GaN HEMT device while Fig.6(b) is the output voltage and current waveform using the Si MOS device. It can be seen that the output of the totem-pole PFC circuit using the GaN HEMT devices provides less ripple and more stable compared to the Si MOS devices.

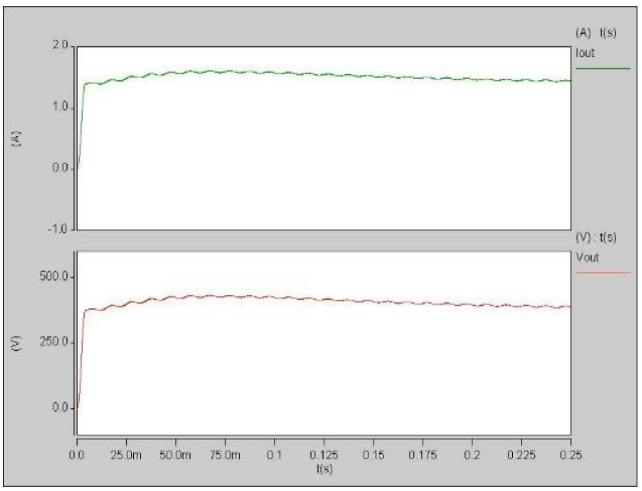

(a)

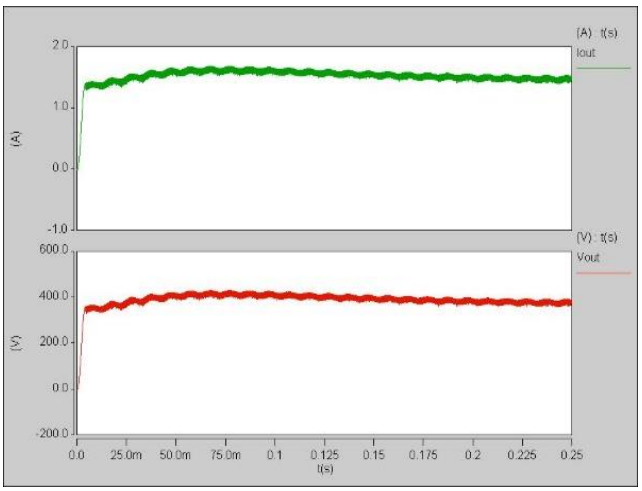

(b)

Fig. 6 The totem-pole bridgeless PFC circuit output voltage and current waveforms: (a) GaN HEMT device and (b) Si MOS device

According to the LLC resonant circuit outputs, Fig.7(a) shows the output voltage and current waveforms using GaN HEMT devices while Fig.7(b) shows the output voltage and current waveforms using Si MOS devices, V_{rms}=48.795V, I_{rms}=10.589A when using GaN HEMT devices, V_{rms}=48.577V and I_{rms}=10.577A when using Si MOS devices. It can be seen that the two types of output waveforms in the LLC resonant circuit are basically the same when the resonant frequency is not high. The highest efficiency is 97.5% in simulation experiments.

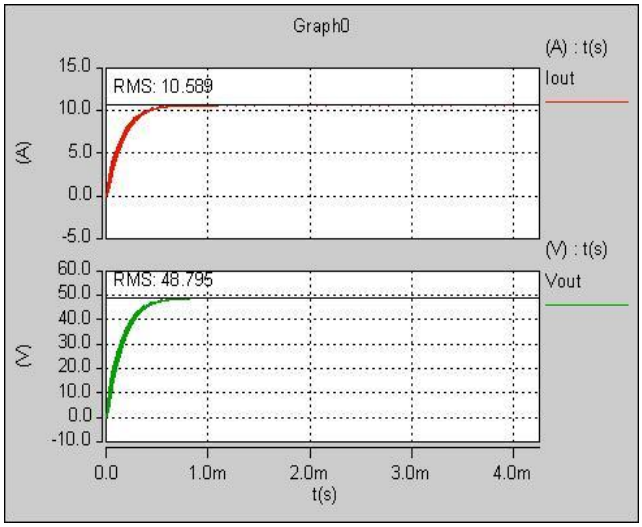

(a)

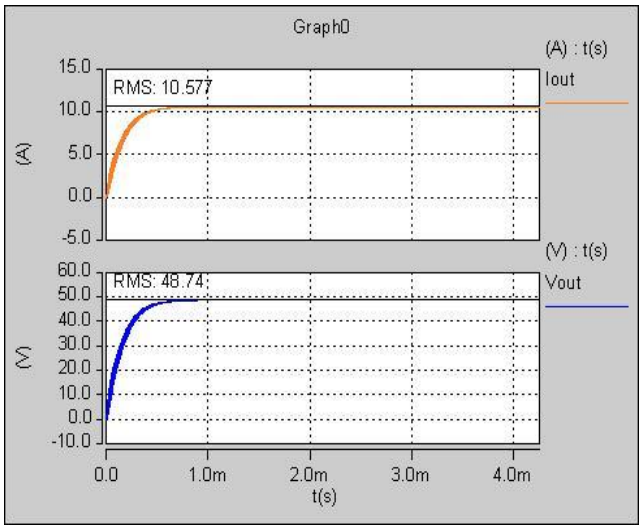

(b)

Fig. 7 The current and voltage waveforms of the LLC resonant circuit when using: (a) GaN HEMT devices and (b) Si MOS devices

5.2 Comparison of Voltage and Current Stresses on Semiconductor Devices

Fig. 8(a) and Fig.8(b) show the current and voltage waveforms on the semiconductor devices of the totem-pole bridgeless PFC circuit when using the GaN HEMT devices and Si MOS devices, respectively. Since the GaN HEMT devices has no body diode problem, it can be seen that the peak reverse recovery current of the PFC circuit of the GaN-based devices is I_{peak}=-6.8595A, while that of the Si-based device is I_{peak}=-144.98A. This shows that GaN-based devices provide significant less voltage and current stress on the circuit elements than Si-based devices.

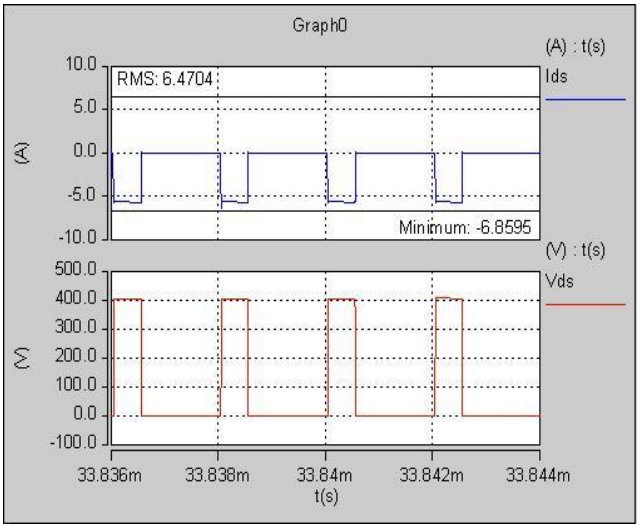

(a)

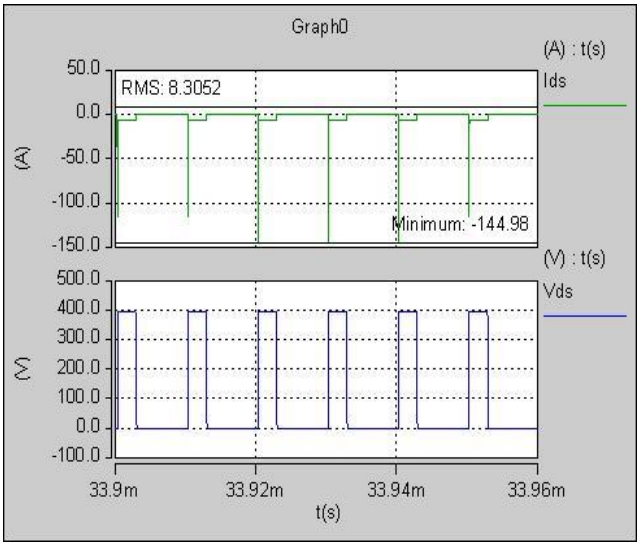

(b)

Fig. 8 The current and voltage on the semiconductor devices of the totem-pole bridgeless PFC circuit when using: (a) GaN HEMT devices and (b) Si MOS devices

Fig. 9(a) and Fig. 9(b) show the current and voltage waveforms on the semiconductor devices of the LLC resonant circuit when using the GaN HEMT devices and the Si MOS devices, respectively. When using the GaN HEMT devices, V_{peak}=385.63V, I_{peak}=-5.5811A, while using the Si MOS devices yeilds V_{peak}= 385.22V, I_{peak}= -5.5825A, it can be seen that in the LLC resonant circuit, the current and voltage stresses of GaN HEMT and Si MOS are basically the same.

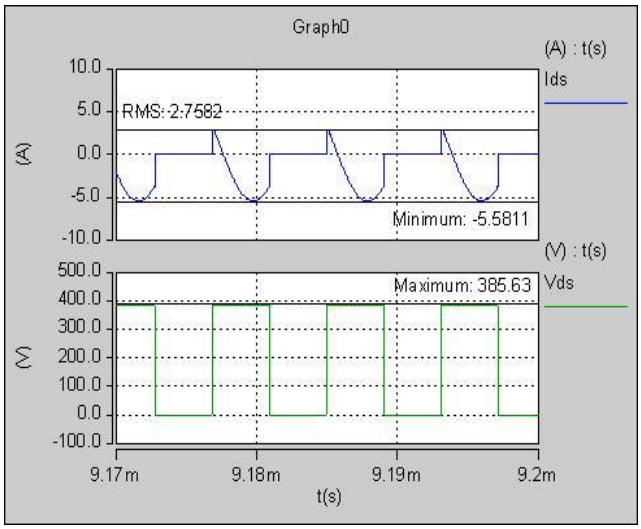

(a)

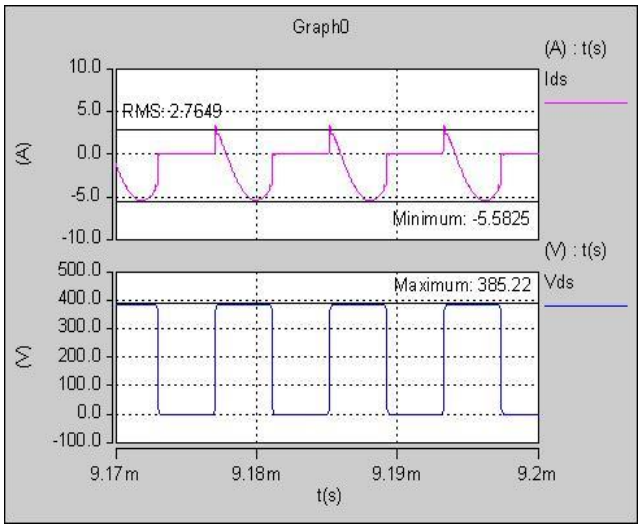

(b)

Fig. 9 The current and voltage waveforms on the semiconductor devices of the LLC resonant circuit when using: (a) GaN HEMT devices and (b) Si MOS devices

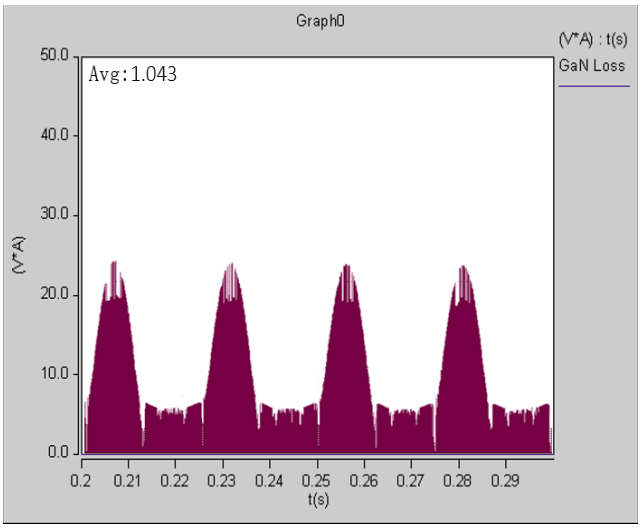

(a)

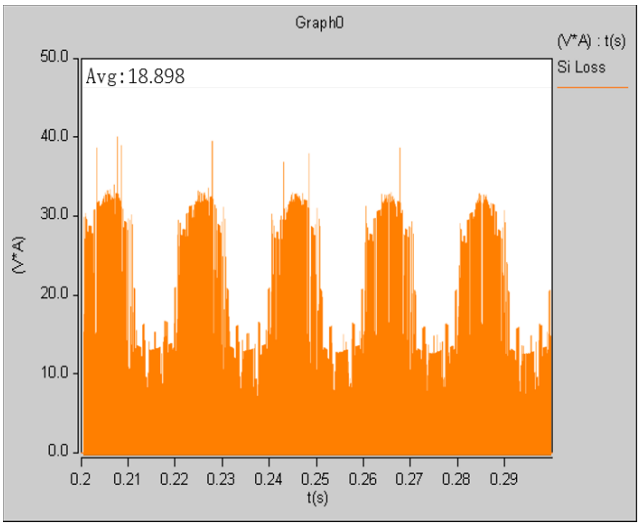

(b)

Fig. 10 The power loss waveform of the totem-pole bridgeless PFC circuit when using: (a) GaN HEMT devices and (b) Si MOS devices

5.3 Comparison of Losses

The main losses of the power supply include devices' conduction loss, turn-off switching loss, inductor core loss, and winding loss, etc. This section only compares the conduction loss, turn-off switching loss of GaN HEMT devices and Si MOS devices. Fig. 10(a) and Fig. 10(b) show the power loss of the totem-pole bridgeless PFC circuit when using the GaN HEMT devices and the Si MOS devices. The circuit with the GaN HEMT devices provided average loss of 1.043 W while the circuit with the Si MOS devices provided 18.898 W. The loss of Si MOS devices is approximately 18 times higher than that of the GaN HEMT devices.

On the other hand, When consider the power losses of the LLC resonant circuit, the resultant power loss waveforms would be ones shown in Fig.11(a) and Fig.11(b). Fig.11(a) shows the power loss waveform when the GaN HEMT devices were used while Fig.11(b) shows the waveform when the Si MOS devices were used. It can be seen that the average loss for the GaN HEMT is 1.961 W while the Si MOS is 3.089 W. It is clearly seen that the power loss of the LLC circuit when using the GaN HEMT devices is only 63.5% of that of Si MOS devices. It is noted that the power losses dissipated from the LLC circuit has small different compared to the totem-pole bridgeless PFC circuit. This is because of the fact that the soft switching approach was used. Fig. 13 shows the comparison of the power losses between the GaN HEMT devices and Si MOS devices.

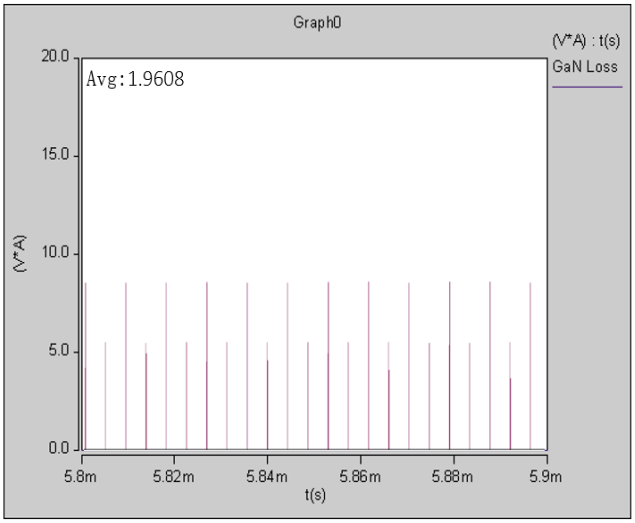

(a)

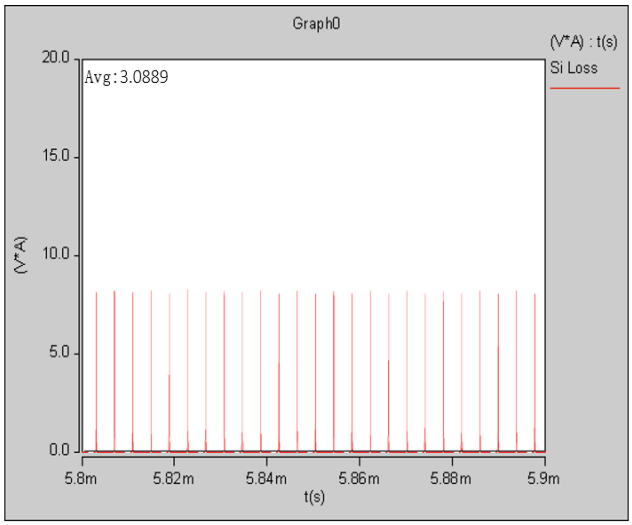

(b)

Fig. 11 Power loss of the LLC resonant circuit when using: (a) GaN HEMT devices and (b) Si MOS devices

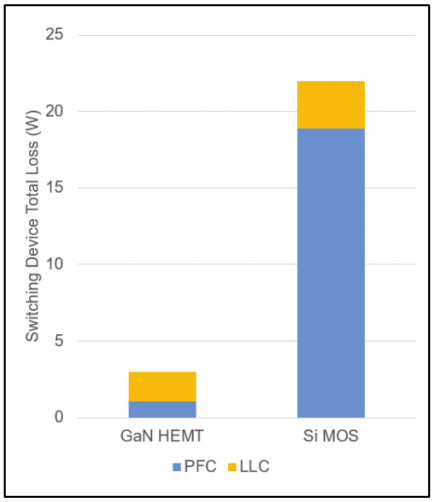

Fig. 13 Comparison of the power losses on the proposed power supply circuit between the GaN HEMT devices and the Si MOS devices

5.4 Comparison of Efficiency

Fig. 14 shows the comparison of the efficiency of the proposed robot power supply of a totem-pole bridgeless PFC converter with a LLC resonant circuit when using the GaN HEMT devices and the Si MOS devices for different load levels between 120-500W. The GaN-based circuit achieved higher efficiency (95.1-97.5%) for the whole range of the considering load levels than the Si-based circuit (91.1-95.3%). The GaN-based circuit achieved the highest efficiency of 97.5% at 260W while the Si-based only 95.3% at 330W. The GaN-based circuit could improve the efficiency by 2.7% compared to Si-based circuit.

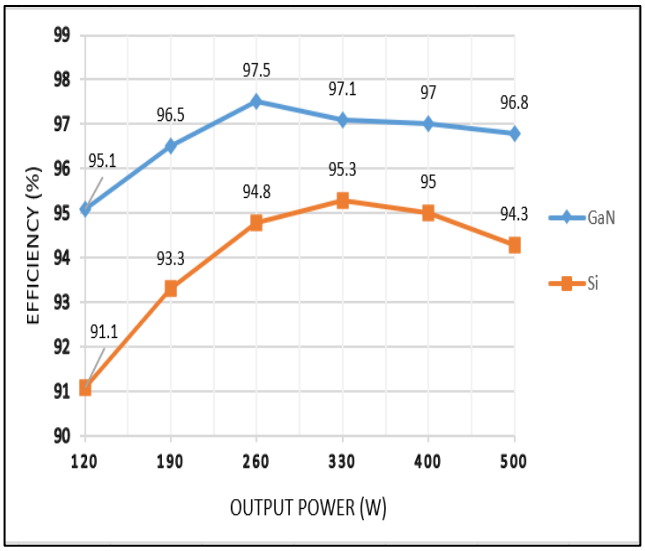

Fig. 14 Comparison of efficiency of the proposed robot power supply using the totem-pole bridgeless PFC converter with a LLC resonant circuit when using the GaN HEMT devices and Si MOS devices

6. Conclusions

The utilization of the GaN HEMT semiconductor devices to achieve higher efficiency, more reliability, and higher power density robot power supply compared to conventional Si MOS devices has been proposed in this paper. Design for a high frequency (500 kHz) single phase bridgeless PFC with a LLC resonant circuit to achieve high efficiency. The highest efficiency of 97.5% could be achieved by the GaN-based converter while the Si-based converter reached only at 95.3% from the simulation experiments. This implies that the GaN-based circuit could provide more suitable for power converter applications than the Si-based circuit.

References

[1] C. C. R. Yeh, C. C. J. Wong, W. W. V. Chang, and C. C. S. Lai, "Labor Displacement in Artificial Intelligence Era: A Systematic Literature Review," (in English), *Taiwan J. East Asian Stud.*, Review vol. 17, no. 2, pp. 25-75, Dec 2020, doi: 10.6163/tjeas.202012_17(2).0002.

[2] K. Jeebkaew, C. Photong, and N. Pannucharoenwong, "Power Quality Improvement for a Single Phase Solar Inverter using a Current Source Inverter with a Buck Converter," *Solid State Technology*, vol. 63, no. 6, pp. 7137-7152, 2020.

[3] T. Deguchi, T. Kikuchi, M. Arai, K. Yamasaki, and T. Egawa, "High On/Off current ratio p-InGaN/AlGaN/GaN HEMTs," *IEEE Electron Device Lett.*, Article vol. 33, no. 9, pp. 1249-1251, 2012, Art no. 6248156, doi: 10.1109/LED.2012.2204854.

[4] G. Greco, F. Iucolano, and F. Roccaforte, "Review of technology for normally-off HEMTs with p-GaN gate," *Materials Science in Semiconductor Processing*, Review vol. 78, pp. 96-106, 2018, doi: 10.1016/j.mssp.2017.09.027.

[5] N. Kim, J. Yu, W. Zhang, R. Li, M. Wang, and W. T. Ng, "Current Trends in the Development of Normally-OFF GaN-on-Si Power Transistors and Power Modules: A Review," *Journal of Electronic Materials*, Article vol. 49, no. 11, pp. 6829-6843, 2020, doi: 10.1007/s11664-020-08284-7.

[6] M. Kuzuhara and H. Tokuda, "Low-loss and high-voltage III-nitride transistors for power switching applications," *IEEE Transactions on Electron Devices*, Article vol. 62, no. 2, pp. 405-413, 2015, Art no. 6967816, doi: 10.1109/TED.2014.2359055.

[7] M. Meneghini, G. Meneghesso, and E. Zanoni, "Power GaN Devices," *Cham: Springer International Publishing*, 2017.

[8] U. K. Mishra, P. Parikh, and Y. F. Wu, "AlGaN/GaN HEMTs - An overview of device operation and applications," *Proceedings of the IEEE*, Article vol. 90, no. 6, pp. 1022-1031, 2002, doi: 10.1109/JPROC.2002.1021567.

[9] R. Quay, *Gallium nitride electronics*. Springer Science & Business Media, 2008.

[10] F. Ren and J. C. Zolper, *Wide energy bandgap electronic devices*. World Scientific, 2003.

[11] Y. Liu, Z. Ouyang, and M. A. E. Andersen, "Review of soft-switching high-frequency GaN-based single-phase Bridgeless Rectifier," in *2021 IEEE Workshop on Wide Bandgap Power Devices and Applications in Asia (WiPDA Asia)*, 25-27 Aug. 2021 2021, pp. 411-416, doi: 10.1109/WiPDAAsia51810.2021.9656073.

[12] Z. Chen, P. Davari, and H. Wang, "Single-Phase Bridgeless PFC Topology Derivation and Performance Benchmarking," *IEEE Trans. Power Electron.*, vol. 35, no. 9, pp. 9238-9250, 2020, doi: 10.1109/TPEL.2020.2970005.

[13] L. Huber, Y. Jang, and M. M. Jovanović, "Performance evaluation of bridgeless PFC boost rectifiers," *IEEE Trans. Power Electron.*, Article vol. 23, no. 3, pp. 1381-1390, 2008, doi: 10.1109/TPEL.2008.921107.

[14] F. Musavi, W. Eberle, and W. G. Dunford, "A high-performance single-phase bridgeless interleaved PFC converter for plug-in hybrid electric vehicle battery chargers," *IEEE Transactions on Industry Applications*, Article vol. 47, no. 4, pp. 1833-1843, 2011, Art no. 5771100, doi: 10.1109/TIA.2011.2156753.

[15] L. Bing, L. Wenduo, L. Yan, F. C. Lee, and J. D. v. Wyk, "Optimal design methodology for LLC resonant converter," in *Twenty-First Annual IEEE Applied Power Electronics Conference and Exposition, 2006. APEC '06.*, 19-23 March 2006 2006, p. 6 pp., doi: 10.1109/APEC.2006.1620590.

[16] D. Huang, S. Ji, and F. C. Lee, "Matrix transformer for LLC resonant converters," in *2013 Twenty-Eighth Annual IEEE Applied Power Electronics Conference and Exposition (APEC)*, 17-21 March 2013 2013, pp. 2078-2083, doi: 10.1109/APEC.2013.6520582.

[17] W. Zhang, Y. Cui, F. Wang, L. M. Tolbert, B. J. Blalock, and D. J. Costinett, "Investigation of Gallium Nitride devices benefits on LLC resonant DC-DC converter," in *2015 IEEE Applied Power Electronics Conference and Exposition (APEC)*, 15-19 March 2015 2015, pp. 146-153, doi: 10.1109/APEC.2015.7104345.

[18] W. Zhang, F. Wang, D. J. Costinett, L. M. Tolbert, and B. J. Blalock, "Investigation of Gallium Nitride Devices in High-Frequency LLC Resonant Converters," *IEEE Trans. Power Electron.*, vol. 32, no. 1, pp. 571-583, 2017, doi: 10.1109/TPEL.2016.2528291.

[19] M. D. Seeman, S. R. Bahl, D. I. Anderson, and G. A. Shah, "Advantages of GaN in a high-voltage resonant LLC converter," in *2014 IEEE Applied Power Electronics Conference and Exposition - APEC 2014*, 16-20 March 2014 2014, pp. 476-483, doi: 10.1109/APEC.2014.6803351.

[20] L. A. D. Ta, N. D. Dao, and D. Lee, "High-Efficiency Hybrid LLC Resonant Converter for On-Board Chargers of Plug-In Electric Vehicles," *IEEE Trans. Power Electron.*, vol. 35, no. 8, pp. 8324-8334, 2020, doi: 10.1109/TPEL.2020.2968084.

[21] R. Beiranvand, B. Rashidian, M. R. Zolghadri, and S. M. H. Alavi, "Using LLC Resonant Converter for Designing Wide-Range Voltage Source," *IEEE Trans. Ind. Electron.*, vol. 58, no. 5, pp. 1746-1756, 2011, doi: 10.1109/TIE.2010.2052537.

[22] L. Xue., Z. Shen., D. Boroyevich., and P. Mattavelli., "GaN-based high frequency totem-pole bridgeless PFC design with digital implementation," in *2015 IEEE Applied Power Electronics Conference and Exposition (APEC)*, 15-19 March 2015 2015, pp. 759-766, doi: 10.1109/APEC.2015.7104435.

[23] Z. Liu, F. C. Lee, Q. Li, and Y. Yang, "Design of GaN-Based MHz Totem-Pole PFC Rectifier," *IEEE J. Emerg. Sel. Top. Power Electron.*, vol. 4, no. 3, pp. 799-807, 2016, doi: 10.1109/JESTPE.2016.2571299.

[24] "LMG341xR070 600-V 70-mΩ GaN with Integrated Driver and Protection datasheet (Rev. F)," may 2020 ed, 2020.

[25] "Datasheet IPB60R070CFD7," 5-2019 ed, 2019.

Biographies

Jie Gan was born in NanNing, GuangXi, China. He received his Bachelor degree from Chengdu University of Information Technology in 2015. His research interests include robotics, power electronics and power supply applications.

Mohd Azli Bin Salim, Ir. Ts. Dr. received his Ph.D. in Mechanical Engineering majoring in Vibration Engineering. Currently, he obtained the TRIZ Level 3 Practitioner Certificate and Certified Instructor for TRIZ Level 1. In addition, he holds a Professional Engineer (Ir.) from Board of Engineers, Malaysia, and Professional Technologist (Ts.) awarded from Malaysia Board of Technologist. He also awarded as a Chartered Engineer from Institution of Mechanical Engineers and professional registration with Engineering Council, UK. He has also Graduate Member from Board of Engineers, Malaysia, Secretary of Persatuan Penyelidik Pencirian Bahan Termaju, Member of International Association of Engineers and etc. His research interest includes vibration and acoustic analysis, advanced materials, nanotechnology

and nano-composites. He also received "Most Cited Paper from Praise Worthy Prize Publication Indexed by SCOPUS". Recently, he is an author in Materials Science and Materials Engineering module published by Elsevier. Dr. Azli published more 100 international journals published in various indexing include Thomson Reuters and Scopus.

Chonlatee Photong received his B.Eng. from Khon Kaen University, Thailand, in 2001. He worked at Sony Device Technology (Thailand) Co., Ltd. and Seagate Technology (Thailand) Co., Ltd. for 3 and 2 years, respectively, during 2002-2005. He received his M.Sc. in Power Electronics and Drives and Ph.D. in Electrical and Electronic Engineering from University of Nottingham, UK, in 2007 and 2013, respectively. He is currently the bachelor program director of Practical Engineering (Continuing Program) and a lecturer in Power Electronics and Drives at the Faculty of Engineering, Mahasarakham University, Thailand. He is also the head of the Electric Automotive and Energy Technology Research Unit, the Faculty of Engineering, Mahasarakham University, Thailand. He is the member of IEEE-Industrial Society and Power and Energy Society. His research interests include power electronics, power converters for renewable energy conversion, electrical machines and drives, electric vehicles, automotive engineering and energy technologies.